The International Journal of Advanced Manufacturing Technology
https://doi.org/10.1007/s00170-023-11318-z

ORIGINAL ARTICLE

A feasibility study of promoting osseointegration surface roughness by micro-milling of Ti-6Al-4V biomedical alloy

Cristian Cappellini[1] · **Alessio Malandruccolo**[2] · **Andrea Abeni**[3] · **Aldo Attanasio**[3]

Received: 14 November 2022 / Accepted: 23 March 2023
© The Author(s) 2023

Abstract
The reliability of a prosthetic implant needs durability, biocompatibility, and osseointegration capability. Accomplishing these characteristics, Ti-6Al-4V alloy is the main used material for implant fabrication. Moreover, it can be processed by additive manufacturing technique, permitting to meet the needs of patience-tailored, often complex shaped, prosthesis topologies. Once an implant is realized, it is finished by machining operations and its osseointegration capability is heavily influenced by the resulting surface roughness. Consequently, the assessment of this latter is mandatory to evaluate the prosthesis durability. This paper presents the analysis of surface roughness of Ti-6Al-4V micro-milled specimens produced by plastic deformation, selective laser melting, and electron beam melting processes. A central composite design was employed for planning the cutting tests. The comparison between surface roughness results and its values for enhancing osseointegration, firstly permitted to individuate the range of micro-milling suitable applications, which have been individuated as ball joints, bone plates, and screws. Next, the statistical analysis of the experimental measurements allowed the identification of the most influential micro-milling parameters together with the determination of the mathematical models of surface roughness by response surface methodology. The good comparison among calculated and experimental results revealed the reliability of the model, allowing the prediction of achievable surface roughness once micro-machining parameters are selected, or their optimization as a function of a desired surface roughness value.

Keywords Ti-6Al-4V · Osseointegration · Surface roughness · Micro-milling · Additive manufacturing · ANOVA

1 Introduction

The extension of human life expectancy in our era has led to an increase in the demand for artificial implants in dental and orthopaedical field, with a predicted request of only hip and knee implants revisions of 3.48 billion by 2030; as underlined in the work of Sarraf et al. [1]. Moreover, Hao et al. [2] observed that prostheses are required to endure in the human body, without accomplishing failures, for a long time. Hence, to ensure this durability, Heimann [3] found that prosthesis materials must possess, at the same time, several characteristics, such as the extreme resistance to corrosive phenomena typical of a living environment with aggressive, often changing conditions, as in the human body. Moreover, good wear and fatigue resistance, high strength together with low density and elastic modulus are required [4]. Focusing on metallic biocompatible materials, the most employed are stainless steels, cobalt-chromium, and titanium alloys. Amongst these latter, Ti-6Al-4V was indicated

✉ Cristian Cappellini
cristian.cappellini@unibg.it

Alessio Malandruccolo
alessio.malandruccolo@unibz.it

Andrea Abeni
andrea.abeni@unibs.it

Aldo Attanasio
aldo.attanasio@unibs.it

[1] Department of Management, Information and Production Engineering, University of Bergamo, Via Pasubio 7/b, 24044 Dalmine, Bergamo, Italy

[2] Faculty of Science and Technology, Free University of Bolzano, Piazza Università 1, 39100 Bolzano, Italy

[3] Department of Industrial and Mechanical Engineering, University of Brescia, Via Branze 38, 25123 Brescia, Italy

Published online: 28 March 2023

by Aghili et al. [5] as the most widely used for biomedical applications, in particular for joints and bones replacement, and dental implants. The high degree of diffusion of Ti-6Al-4V alloy in biomedical field is due to the combination of its biocompatibility, corrosion resistance and mechanical properties. Considering the need of patience-tailored implant design, AM results to be of great and strategic importance. This technology, in fact, allows to produce specific implants having optimized shapes [6], porosity ratios [7], and bone-comparable elasticity modulus able to profitably interact with the body, helping cells growth and osseointegration, at relatively low costs [8]. Selective laser melting (SLM) and electron beam melting (EBM), both belonging to the powder bed fusion (PBF) methodology, have been revealed by the study of Tong et al. [9] as the most adopted AM techniques to manufacture Ti-6Al-4V components. SLM exploits the thermal power of a laser source to melt powder particles, while the heating source in EBM is an electron beam. Due to this difference, SLM is performed in an inert gas (Ar or He) environment at room temperature with higher powers than EBM process, that is carried out in vacuum at high temperatures. Consequently, SLM is characterized by the use of lower particle sizes and printing speeds, and higher cooling rates with respect to EBM, resulting in different microstructures, tensional states, mechanical properties, and surface qualities [10]. More in detail, SLM products have smaller grain size, elongation percentage, surface roughness, and higher residual stress, ultimate tensile stress than the EBM ones [2]. Even if AM is considered a net-shape process, research conducted by Abeni et al. [11] and Filiz et al. [12] unveiled the requirement of finishing operations to remove surface defects related to lack of fusion and not-melted metallic particles. Amongst finishing processes, as indicated by Huo and Cheng [13], micro-milling (MM) is proficiently employed in medical implant field due to its ability of achieving small and complex shapes. For assessing a good osseointegration, implant surface roughness value is of fundamental importance. Moreover, depending on the typology of the implant, surface roughness must meet specific values [14]. As an example, Albrektsson and Wennerberg [15] determined that for dental implants the value of the roughness parameter S_a should be in the range of 1–2 μm. However, beside the surface roughness influence on osteointegration, other key parameters must be evaluated for ensuring the implant permanency in the body for a long time, such as fatigue, wear, and corrosion resistances [16]. In order to give better explanation related to what has just been mentioned, Fig. 1 highlights a qualitative comparison of the required surface roughness values according to the material use for each one of the three specific applications reported, i.e., dental implants, bone plates and screws, and ball joints. In addition to the required level for surface roughness value

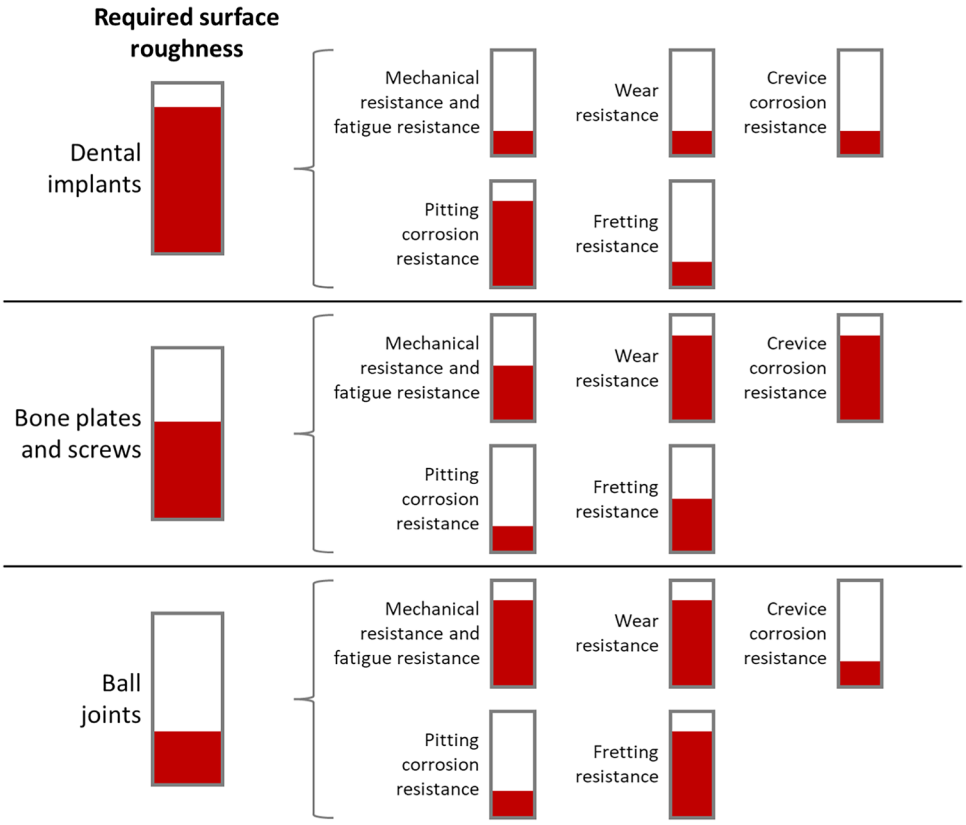

Fig. 1 Qualitative representation of surface roughness levels required for optimal use in the three main applications requiring osseointegration: dental implants, bone plates and screws, ball joints. In addition to surface roughness, the levels of five key requirements that the implant must possess and that may be directly affected by surface roughness, or that may affect its value, are given. Note that the minimum values for each feature do not correspond to zero

for optimal operation and osseointegration, five key requirements for the specific application are given. The five parameters absolutely must be considered for a successful application of the material. Furthermore, they have influence on the optimal value of surface roughness but are themselves influenced by it. In fact, high surface roughness values will be reflected in lower resistance to wear and fretting, as is the case with dental implants. On the other hand, high resistance to fretting will have to pass through low surface roughness values in order to limit the degenerative phenomenon itself and the formation of debris. Not only that, some of these five additional parameters pose interesting challenges to product development as they seemingly conflict with the required surface roughness value. For instance, the requirement for high pitting resistance is apparently at odds with high surface roughness as it is known that polished finish surfaces in alloys that show passivity lead to lower susceptibility to pitting and a lower pit growing rate than rougher surfaces [17]. This implies the need for additional strategies that can increase pitting resistance and that do not rely on a better surface finishing. In order to be able to achieve this goal, it is necessary to analyze all variables involved in osseointegration and that may influence the surface roughness value, so as to effectively define the best strategy. In order to give an indication of the complexity involved, Fig. 2 gives a summary of influencing parameters on optimal S_a for osseointegration.

As already mentioned, an optimal surface roughness value for implant osseointegration has not yet been well defined, and this is due to the complexity of osseointegration mechanism depending again on the application typology (see also Fig. 2) [18]. Moreover, literature data and publications related to this topic do not indicate precise and unambiguous values. This seems to be largely caused by the fact that there is still no standardized approach to surface characterization and in defining the key parameters to be used [14]. Considering of all the previously presented aspects, the study of the MM resulting surface roughness value is mandatory for evaluating the applicability of this finishing process to promote good osseointegration.

Hence, this paper deals with the analysis of the achievable surface roughness in MM of Ti-6Al-4V additively manufactured specimens, by varying cutting parameters. To accomplish this, the experimental measurements of three-dimensional surface roughness S_a [19] were performed. The examination of these results, firstly permitted to individuate which medical applications, that are surface roughness dependent [14], are suitable for MM. The choice of analyzing the S_a three-dimensional roughness parameter (ISO 25178) instead of the R_a one, was related to a lower influence of measurement noise and scratches on S_a than R_a [20] and to a characterization of the height distribution in combination with spatial parameter that led to an improved description of implant surfaces [14, 21]. Secondly, following the need of standardizing evaluation and methodology techniques [14], S_a values were statistically investigated by ANOVA to identify the most influencing parameters, letting the development of reliable mathematical models for S_a estimation. In this manner, the prediction of S_a as a function of the adopted process parameters, or their optimization once the desired S_a value is established, can be achieved. The usage of the developed mathematical models represents a preliminary step on the methodology normalization path, permitting to establish the suitability of MM finishing for a determined medical application, depending on the calculated S_a value, and reducing, at the same time, costly and time-consuming experimental tests.

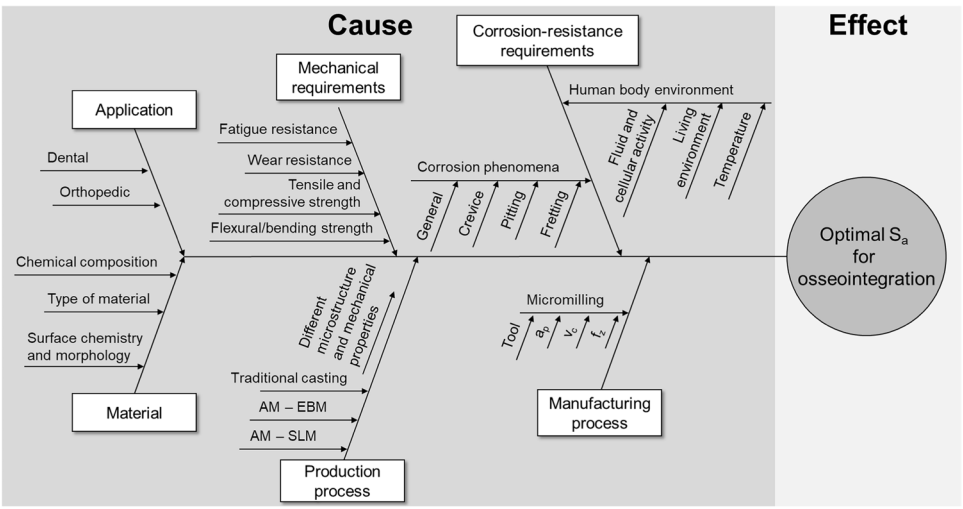

Fig. 2 Summary of influencing parameters on optimal S_a for osseointegration

2 Materials and methods

In order to obtain a sufficient amount of data for a robust statistical analysis, an extensive experimental campaign of micro-milling of differently manufactured Ti-6Al-4V specimens was accomplished. Before going into the details of the specimen preparation procedure, it is worth spending a few words on the specific characteristics of the selected alloy that can be related to the specific field of application, i.e., prosthesis fabrication. Ti-6Al-4V is classified as an α + β alloy, due to a microstructure characterized by the presence of two different structures: α and β. The α-phase is characterized by a hexagonal close-packed (hcp) structure; this leads to good mechanical properties with some limitations for what concerns formability and toughness as direct consequence of the limited number of slip systems characterizing the hcp unit cell. On the other hand, the β-phase shows a body-centered cubic (bcc) structure characterized by a better attitude to undergo plastic deformation thanks to its 12 slip systems. Gialanella and Malandruccolo [22] highlighted that Ti-6Al-4V shows ductility characteristics allowing the production of components with a wide range of technologies, such as forming and additive manufacturing (AM) operations. Ti-6Al-4V is bio-inert, meaning it is able to avoid undesired chemical reactions with body fluids [23]. The alloy possesses a good resistance against general and localized corrosion due to the formation of a protective layer of titanium dioxide (TiO_2), preventing metallic ions release that might lead to inflammatory and allergic reactions [24]. Furthermore, it has the highest strength-weight ratio amongst metallic biomaterials, providing good mechanical resistance together with a correct weight's distribution in human body [25]; it is paramagnetic, reducing complications when undergoing computed tomography (CT) [1]. In addition to this, it owns a relatively low modulus of elasticity slightly above 100 GPa, limiting stress shielding phenomena and the correlated risk of implant loosening under load [3]; it enhances osseointegration by cementless joints since TiO_2 and hydroxyapatite (the bones' material) are both ceramic and their interaction is good, leading to a durable bone-implant anchorage [25]. Finally, it is characterized by a high fatigue strength, mandatory in the cyclic load at which the human body is subjected [3]. However, Herbster et al. [26] demonstrated its sensitivity to fretting corrosion, giving an abrasion of the TiO_2 layer that is faster than its repassivation, increasing its susceptibility to fatigue crack initiation. The first group of Ti-6Al-4V specimens employed consisted of those in the supplied state, hereafter named as-received, of bars with a diameter of 20 mm resulting from a hot plastic deformation process. The second and third groups, were obtained by SLM and EBM additive manufacturing processes respectively, as described by Ginestra et al. [27]. Figure 3 shows the three different microstructures of the materials after polishing and 20 s etching by Kroll's reagent, consisting of 6 ml HNO_3, 2 ml HF in 100 ml of distilled water, in which the white and the dark parts represent α-phase and β-phase, respectively.

For all groups, specimens with a cubic geometry with an edge length of 10 mm were realized. SLM specimens were produced starting from Ti-6Al-4V powders, namely EOS Titanium Ti-6Al-4V, by means of an EOS M290 machine (EOS, Robert-Stirling-Ring 1, D-82152 Krailling Germany), in a controlled argon atmosphere. The employed process parameters were a power of the laser source of 340 W, a laser focus of 70 µm, a scanning speed of 1250 mm/s, a hatch spacing of 40 µm, a slice thickness of 30 µm, and an alternating angle of deposition between layers of 67°. EBM samples were manufactured from ARCAM Ti-6Al-4V powders

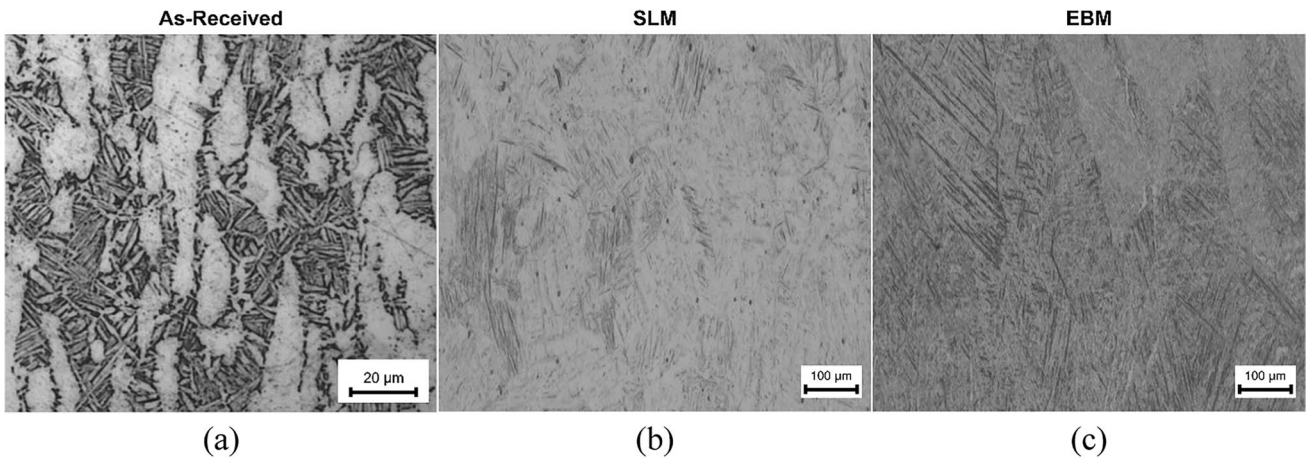

Fig. 3 Ti-6Al-4V microstructure before micromilling for **a** as-received, **b** SLM, and **c** EBM materials

with an EBM SYSTEM MODEL A2 machine (ARCAM, Designvägen 2 SE-435 33 Mölnlycke Sweden), in a vacuum environment. The adopted parameters were a beam power of 1250 W, a focus of 80 µm, a scanning speed of 4530 mm/s, a hatch spacing of 100 µm, a slice thickness of 50 µm, and an alternating angle of deposition amongst layers of 90°. Table 1 gives dimensional and chemical properties of the employed powders. After the AM process, the specimens were sonically cleaned in an acetone-isopropanol solution, and subsequently left dry.

The micro-milling operations were executed by means of a five axis Nano Precision Machining Center KERN Pyramid Nano (Kern Micro Technik, Olympiastr. 2, D-82418 Murnau-Westried Germany) furnished with a Heidenhain iTCN 530 numeric control. With the aim of obtaining a planar surface on which performing the micro-milling process, each specimen was previously roughed by way of a face milling operation with an axial depth of cut of 100 µm by a three flutes flat bottom mill, with a nominal diameter of 3mm, a cutting speed of 100 m/min, and a feed per tooth of 7.5 µm. Following this, the micro-milling tests, consisting in the realization of micro-channels in the central part of the specimen, along the whole length of the edge, were accomplished with a two-flutes micro-mill, RIME HM79/05, with a nominal diameter of 0.5 mm, visible in Fig. 4. The tool was made of sintered tungsten carbide (WC) in a cobalt (Co) matrix, coated with titanium aluminum nitride (TiAlN). Table 2 reports the effective geometrical properties, measured by an optical confocal microscope Hirox RH 2000 (Hirox Co.,Ltd. Tokyo, Japan), of the employed micro-mill.

The realization of micro-channel was performed by keeping a constant value of the axial depth of cut a_p equal to 0.03 mm, as suggested by the technical datasheet of the micro-mill producer and varying the values of cutting speed V_C and feed per tooth f_Z at determined intervals. In particular, the values of cutting speed were varied in a range between 30 and 50 m/min, while the ones related to the feed per tooth in a range between 2.0 and 4.0 µm/tooth*rev, obtaining a central composite design (CCD) experimental plan considering an α value of 2, as applied by Men et al. [28]. The micro-milling test corresponding to the CCD central point, with V_C = 40 m/min and f_Z = 3.0 µm/tooth*rev was repeated three times with the aim of increasing the reliability of the statistical analysis [29]. Figure 5 shows the values of the selected process parameters for each typology of manufacturing process of the specimens. In this manner, 11 machining tests were performed for as-received, SLM, and EBM samples, leading to a total number of 33 experiments.

Table 1 Dimensional and chemical properties of Ti-6Al-4V powders employed in AM specimens' production processes

Particle size [µm]	SLM	EBM
d10	28	50
d50	38	68
d90	96	54
Powder apparent density [g/cm³]	2.31	2.57
Chemical composition [%wt]		
Al	5.92	6.42
V	4.04	3.88
O	0.13	0.13
Fe	0.20	0.18
Ti	Bal.	Bal.

Table 2 Geometrical properties of the tool used for the micro-channels machining

Property	Value
Effective diameter [µm]	475 ± 4
Effective cutting edge radius [µm]	5 ± 2
Helix angle [°]	30

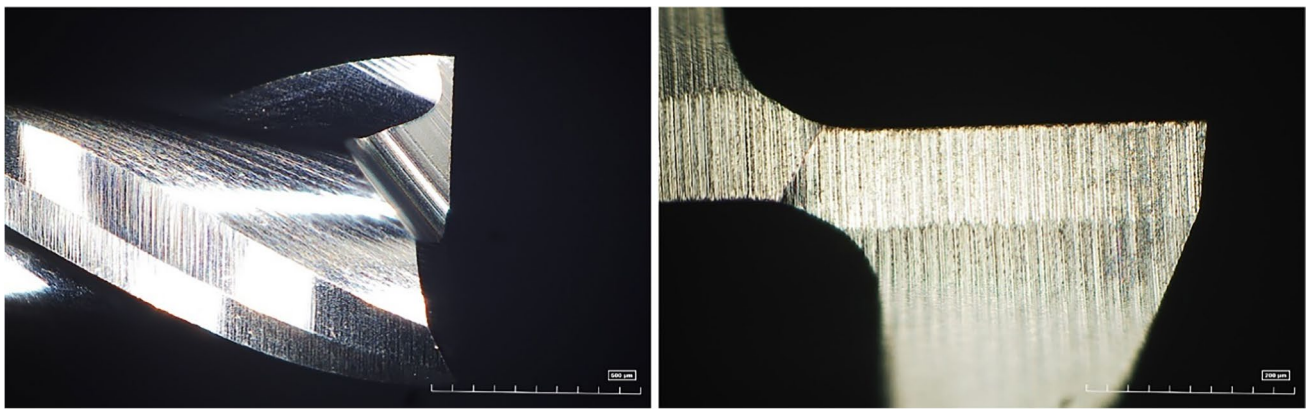

Fig. 4 The RIME HM79/05 tool employed for micro-milling tests

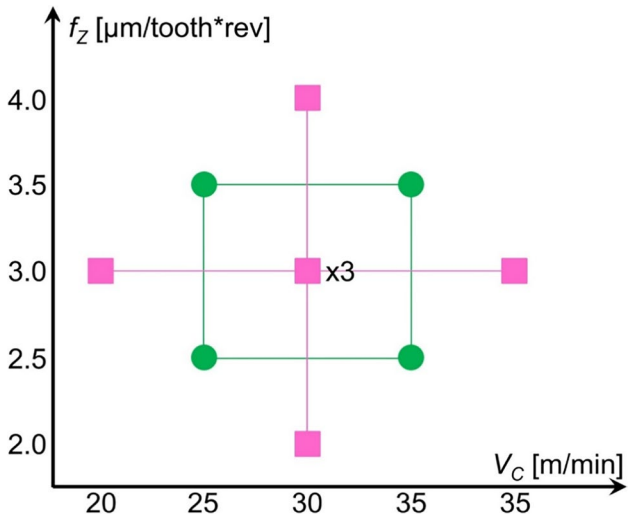

Fig. 5 Summary of the employed micro-milling parameters by the related CCD representation

The cutting speed range was selected according to the values suggested in the manufacturer's datasheet, while the designated range of feed per tooth was bounded to the adopted values because unexpected tool breakage was observed at higher f_Z values.

In order to avoid undesired effects on the final achieved surface related to tool wear occurrence, the tool was substituted after each channel micro-milling.

At the end of each machining test, the three-dimensional surface roughness parameters S_a was measured with the optical microscope Mitaka PF60 (Mitaka Kohki. Co.,Ltd., Japan). According to ISO 25178 standard for three-dimensional parametric definition of surface texture, the mean height of surface irregularities S_a can be calculated using Eq. (1):

$$S_a = \frac{1}{LB}\int_0^L \int_0^B |\eta(x,y)|dxdy \tag{1}$$

where $\eta(x,y)$ is the deviation of the surface irregularities from the base plane, L is the length, and B is the width of the given section of surface. The adopted scanning size for the optical imaging was of 0.245 × 2.3 mm^2 positioned at the central point of the micro-machined surface, with minimum and maximum focusing points of the height of the surface sample, and a magnification of 400×. The image processing for obtaining the S_a values was performed by using the Digital Surf MountainsMap Premium software version 8 (Digital Surf, Besançon, France). Figure 6 depicts an example of the resulting measurement for the SLM specimen machined with $V_C = 40$ m/min and $f_Z = 0.30$ µm/tooth*rev, while in Table 3, the acquired S_a measurements for all the tests are presented.

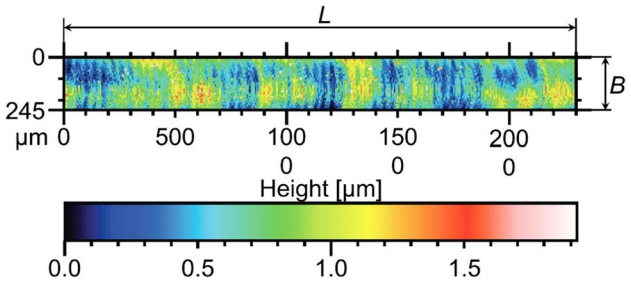

Fig. 6 Example of the acquired S_a measurement ($V_C = 40$ m/min, $f_Z = 30$ µm/tooth*rev)

3 Results and discussion

In order to investigate the effects of the variation in process parameters, and which ones are the most impactful, on surface roughness, an analysis of variance (ANOVA) of S_a values was performed for the three cases, namely as-received, SLM, and EBM. The reliability of the results analysis, and the related derived regression models, is strictly correlated to their normality [30]. Hence, in order to check the normal distribution of the acquired S_a data, their probability plots, in which the percentage of the normal probability of the data residuals are represented, were computed (Fig. 7). Referring to these plots, the straight central line represents the cumulative probability, while the two curves highlight the 95 % confidence interval (CI) boundaries. The data respect the normality assumption when they are enclosed between the CI curves and closely positioned to the cumulative probability line.

The probability plots of as-received (Fig. 7 a) and EBM (Fig. 7 c) S_a values are in accordance with the previously presented normality definition, while SLM (Fig. 7 b) ones

Table 3 Summary of the S_a experimental values for all the tests

V_C [m/min]	f_Z [µm/tooth*rev]	As-received S_a [µm]	SLM S_a [µm]	EBM S_a [µm]
40	4.0	0.36	0.20	0.27
45	3.5	0.27	0.20	0.20
35	3.5	0.29	0.22	0.24
50	3.0	0.27	0.20	0.25
40	3.0	0.37	0.26	0.26
40	3.0	0.34	0.22	0.34
40	3.0	0.35	0.24	0.29
30	3.0	0.44	0.31	0.25
45	2.5	0.37	0.22	0.25
35	2.5	0.32	0.29	0.29
40	2.0	0.39	0.29	0.23

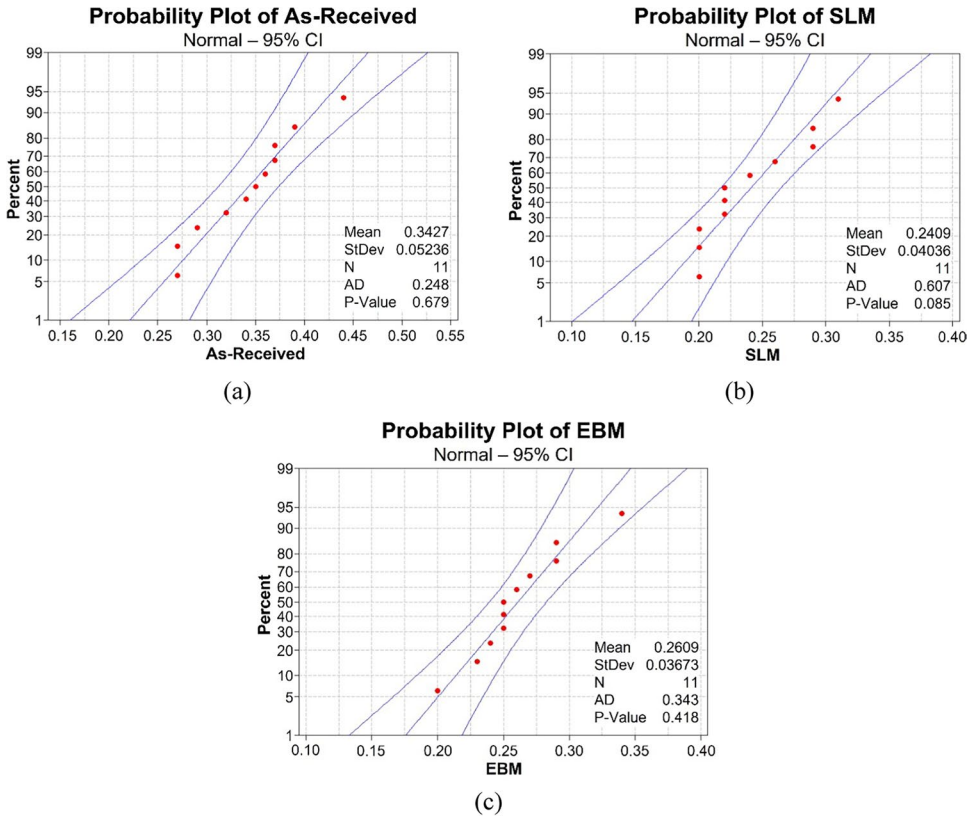

Fig. 7 Probability plots of S_a for **a** as-received, **b** SLM, and **c** EBM specimens

are not normally distributed. Therefore, a normalization of these latter is mandatory. As suggested in [29], a Johnson transformation can be utilized for this purpose. Following this, the SLM S_a values were normalized by the application of Eq. (2):

$$S_{a\_SLMnorm} = 0.392249 + 0.550540 \bullet \ln\left(\frac{S_{a\_SLM} - 0.196534}{0.320174 - S_{a\_SLM}}\right) \quad (2)$$

where S_{a_SLM} are the experimental S_a values, and $S_{a\_SLMnorm}$ are the normalized ones. Figure 8 illustrates that $S_{a\_SLMnorm}$ values are normally distributed, thus the resulting statistical analysis can be considered reliable.

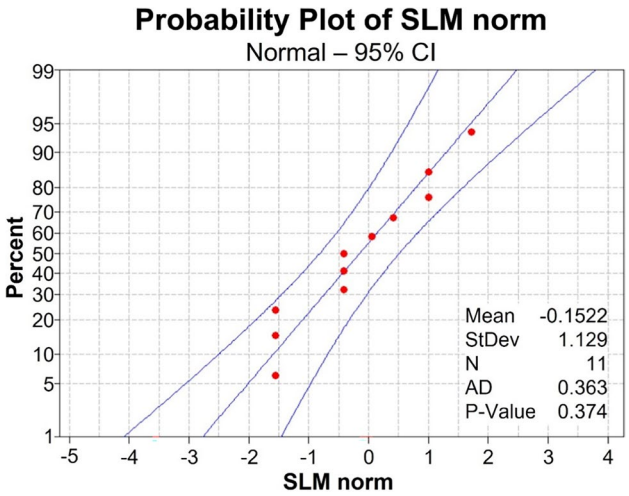

Fig. 8 Probability plots of $S_{a\_SLMnorm}$

3.1 As-received S_a values analysis

The results of the ANOVA for the S_a values of as-received specimens are shown in Table 4. The Source column gives the process parameters that have been analyzed, where it can be seen that not only their individual effects on the surface roughness behavior were considered, but also their interaction and their squared contribution. In the other columns the number of degrees of freedom (DoF) are given for each source, together with, the adjusted sum of squares (Adj. SS), the adjusted mean of squares (Adj. MS), the F-value, and the p value. In the common practice, for assessing if a determined source parameter has a significant influence on the final response, in this case the surface roughness S_a, the p value is the most useful parameter. Whenever the p value is lower than a predefined threshold value, also known as significance level, the null hypothesis H_0, that states that there is no relation between the source and the outcome, is rejected. The significance level for the p-value depends on the CI. Since, for the presented analysis, CI = 95 %, the significance level is equal to 1 – 95 % = 0.05. Consequently,

Table 4 ANOVA results for S_a of as-received specimens

Analysis of variance of S_a for as-received specimens					
Source	DoF	Adj SS	Adj MS	*F* value	*p* value
f_Z	1	0.003008	0.003008	1.05	0.352
V_C	1	0.008008	0.008008	2.80	0.155
$f_Z \times f_Z$	1	0.000852	0.000852	0.30	0.609
$V_C \times V_C$	1	0.000052	0.000052	0.02	0.898
$f_Z \times V_C$	1	0.001225	0.001225	0.43	0.542
Error	5	0.6598	0.13196		
Total	10	12.7408			

Table 5 ANOVA results for S_a of as-received specimens without outlier

Analysis of variance of S_a for as-received specimens without outlier					
Source	DoF	Adj SS	Adj MS	*F* value	*P* value
f_Z	1	0.000057	0.000057	0.16	0.712
V_C	1	0.015858	0.015858	43.93	0.003
$f_Z \times f_Z$	1	0.000600	0.000600	1.66	0.267
$V_C \times V_C$	1	0.000006	0.000006	0.02	0.900
$f_Z \times V_C$	1	0.008901	0.008901	24.66	0.008
Error	4	0.001444	0.000361		
Total	9	0.024360			

if the *p* value is smaller than 0.05, the alternative hypothesis H_1 is considered correct, concluding that there is a statistically significant relation between the source and the outcome [30].

The ANOVA results of Table 4 do not reveal any influence of neither feed per tooth nor cutting speed on micro-machined surface roughness values. In fact, there are no *p*-value lower than 0.05. This first outcome is quite suspicious as unexpected. By ANOVA the presence of an outlier was discovered. An outlier is defined as a value of the response having a standard residual higher than the standard deviation of the other values distribution. It may be either caused by an error in calculation or data coding, or by a measurement error. In the case of outliers having a standard residual higher than 3 times the standard deviations, they can be excluded from the analysis without compromising its significance. The standard residual of the S_a value related to V_C = 35 m/min and f_Z = 3.5 µm/tooth*rev is equal to 2.12, which results to be greater than 3 times the standard deviation of as-received data, equal to 0.05236. Thus, it has been removed from the analysis, and a new ANOVA, whose results are visible in Table 5, was performed.

The ANOVA outcomes of Table 5 underline that cutting speed and its interaction with the feed per tooth variation, significantly affect the evolution of S_a for the as-received material. In particular, as depicted in the main effects plots of Fig. 9, if V_C increases the surface quality is enhanced, meaning that S_a value decreases. The same trend is observable for the variation of f_Z, although a statistical correlation of it with S_a was assessed. The surface and contour plots of Fig. 10 summarize the clear effect of the V_C-f_Z interaction, and again indicate that the way in which f_Z influences S_a is not clear, since at low V_C an increase of f_Z lead to an augmentation of S_a, while at high V_C the inversion of the S_a trend is detected. Considering these outcomes, the f_Z effect needs to be further investigated.

3.2 SLM S_a values analysis

The results of the ANOVA performed on the normalized values of S_a for SLM specimens are summarized in Table 6.

It can be clearly seen that the most affecting parameters on the evolution of S_a values in case of SLM specimens are V_C and f_Z, while their interaction and squared contribution are negligible. A reduction of both V_C and f_Z increases the value of machined surface roughness, as described by the variation trends shown in the main effects plots of Fig. 11. This trend is visible in the related surface and contour plots of Fig. 12 as well.

3.3 EBM S_a values analysis

The ANOVA performed on the surface roughness data obtained from micro-milled EBM specimens yields the results shown in Table 7.

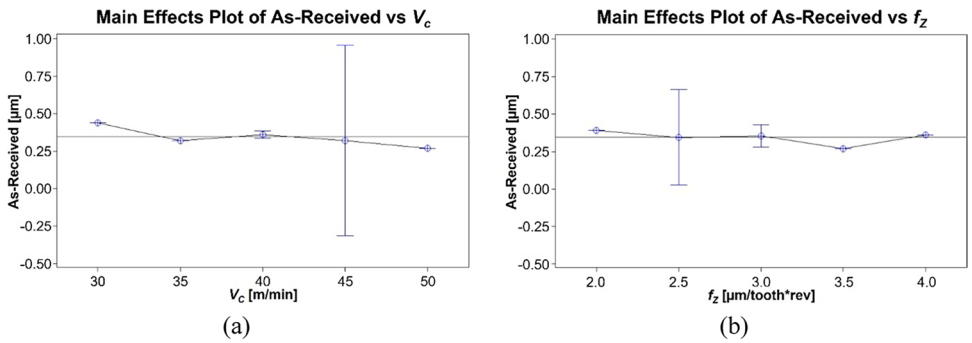

Fig. 9 Main effects plots of as-received S_a respect to **a** V_C and **b** f_Z

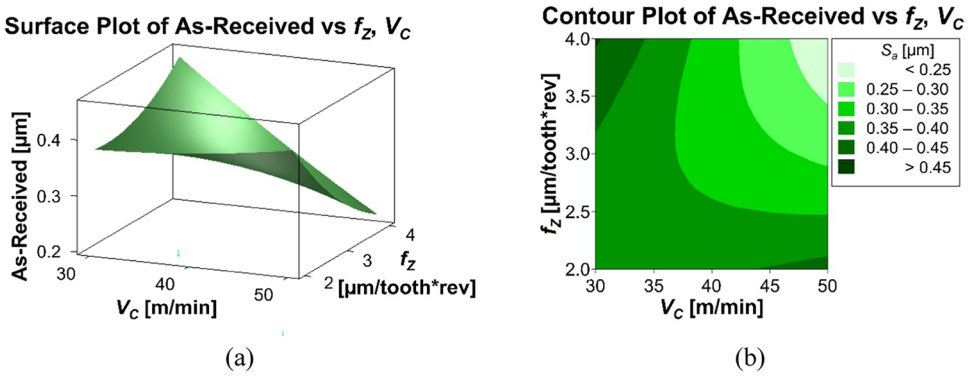

(a) (b)

Fig. 10 **a** Surface and **b** contour plots for as-received S_a

Table 6 ANOVA results for normalized value of S_a for SLM specimens

Analysis of variance of normalized S_a for SLM specimens					
Source	DoF	Adj SS	Adj MS	F value	p value
f_Z	1	4.9718	4.97183	37.68	0.002
V_C	1	6.9535	6.95354	52.69	0.001
$f_Z \times f_Z$	1	0.0841	0.08411	0.64	0.461
$V_C \times V_C$	1	0.0095	0.00947	0.07	0.800
$f_Z \times V_C$	1	0.0180	0.01799	0.14	0.727
Error	5	0.6598	0.13196		
Total	10	12.7408			

The only influencing parameter on the S_a value is the cutting speed. Also in this case, when V_C decreases, surface roughness increases, and this behavior is described by the negative slope of the V_C plot in the main effects diagrams in Fig. 13. Moreover, similar behavior is detectable for the effect of f_Z, but as observed in the case of as-received samples, it has no influence, and its final contribution needs to be further examined. The surface and contour plots of Fig. 14 show the great impact of V_C on S_a for EBM specimens and, in addition, the neglectable effect, especially at higher cutting speed value, of f_Z.

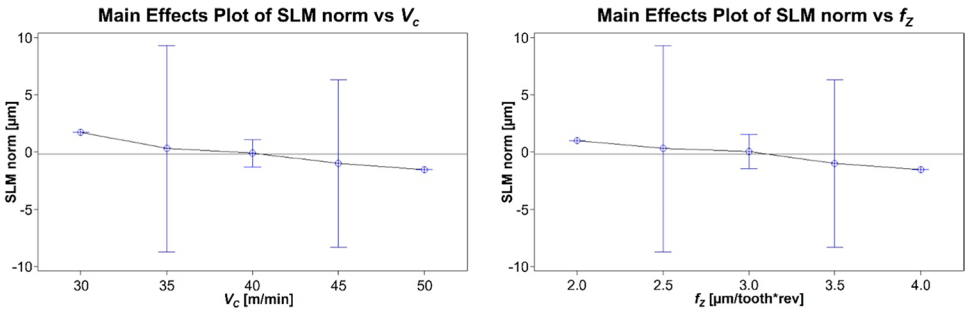

(a) (b)

Fig. 11 Main effects plots of SLM normalized S_a respect to **a** V_C and **b** f_Z

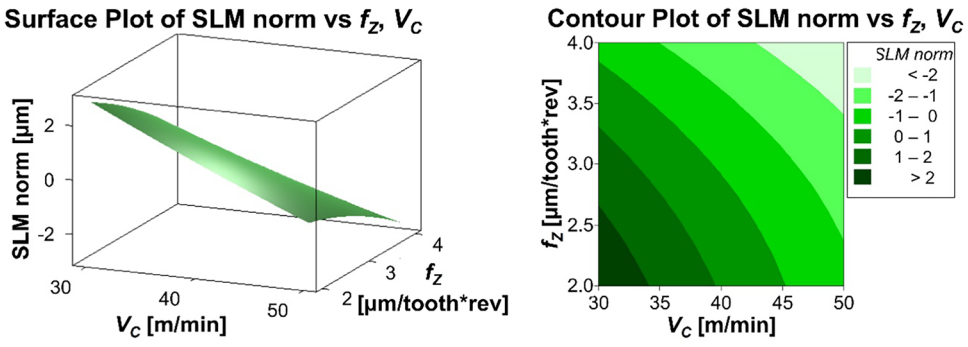

(a) (b)

Fig. 12 **a** Surface and **b** contour plots for SLM normalized S_a

Table 7 ANOVA results of S_a values for EBM specimens

Analysis of variance of S_a for EBM specimens					
Source	DoF	Adj SS	Adj MS	F value	p value
f_Z	1	0.001408	0.001408	3.05	0.141
V_C	1	0.005208	0.005208	11.29	0.020
$f_Z \times f_Z$	1	0.000647	0.000647	1.40	0.290
$V_C \times V_C$	1	0.000056	0.000056	0.12	0.741
$f_Z \times V_C$	1	0.000225	0.000225	0.49	0.516
Error	5	0.6598	0.13196		
Total	10	12.7408			

3.4 RSM regression models

With the intent of analyzing the effects of different micro-milling parameters on the surface roughness value, numerous studies have been developed. A summary of them is reported in Table 8, where the machined workpiece (WP) material, the evaluated roughness parameter (SP), the analyzed micro-milling process parameters (MMP), and the model derivation source are indicated.

Most of the studies of Table 8 had analyzed the behavior of roughness parameter R_a in the case of specimens not produced by AM processes and with different materials respect Ti-6Al-4V investigated in this work. Therefore, to better evaluate the effects of production process type, the development of mathematical models of surface roughness considering this aspect, results to be a profitable task. To develop mathematical models capable of reliably predicting the evolution of micro-milled surface roughness as a function of the variation of the employed machining parameters and the production process, the response surface methodology (RSM) was applied to the experimental measurements of S_a. By means of RSM, a regression model was derived for each type of manufacturing process applied to sample preparation. This methodology conveys to the formulation of Eq. (3), Eq. (4), and Eq. (5) for as-received (S_{a_AR}), SLM normalized ($S_{a\_SLMnorm}$), and EBM (S_{a_EBM}) S_a values, respectively.

$$S_{a\_AR} = 1.9 + 0.79f_Z + 0.060V_c + 0.022f_Z^2 + 0.000023V_c^2 - 0.023f_ZV_c \tag{3}$$

$$S_{a\_SLMnorm} = 12.1 - 0.78f_Z - 0.304V_c - 0.264f_Z^2 + 0.00089V_c^2 + 0.027f_ZV_c \tag{4}$$

$$S_{a\_EBM} = 0.23 - 0.041f_Z + 0.011V_c + 0.023f_Z^2 - 0.000068V_c^2 - 0.003f_ZV_c \tag{5}$$

To check the validity of the regression models obtained, a comparison between the experimental and calculated values was carried out. Due to the Johnson transformation applied to the S_{a_SLM} data, to correctly achieve the parallel, an inverse transformation must be applied to the $S_{a\_SLMnorm}$

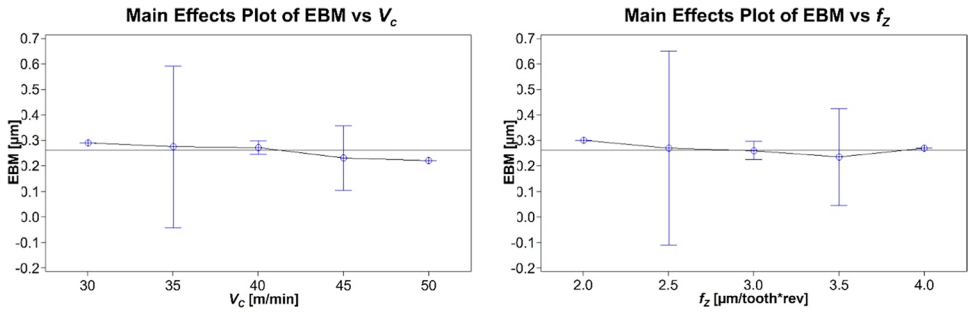

Fig. 13 Main effects plots of EBM S_a respect to **a** V_C and **b** f_Z

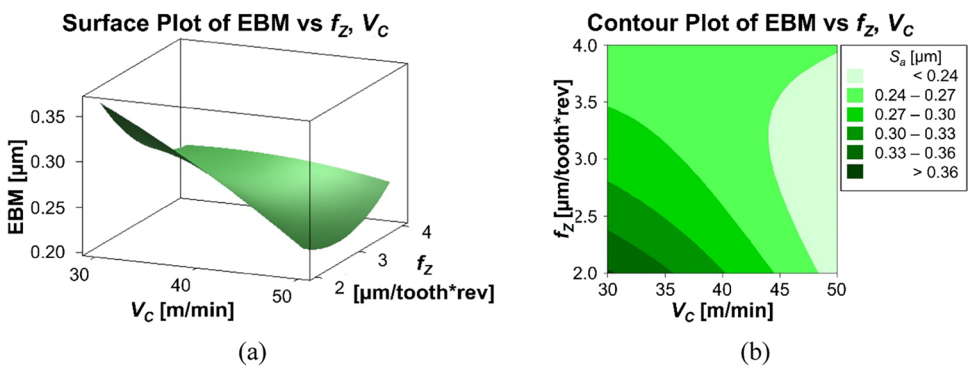

Fig. 14 **a** Surface and **b** contour plots for EBM S_a

Table 8 Summary of studies on surface roughness in micro-milling processes

Ref.	WP material	SP	MMP*	Model source	Comments
[31]	Not declared	R_a	f_Z, *MUCT*	Geometric	Ploughing-shearing transition-based
[32]	OFHC Copper	R_a	f_Z, V_C, *MUCT*, *TRA*, r_e	Geometric	Surface topology representation
[33]	Commercial brass	R_a	f_Z, V_C	No model	
[34]	Al7075, Ti-6Al-4V	R_a	f_Z, V_C, a_p, channel depth, coolant	RSM	2nd order factors' interactions
[35]	AISI 1045	k_C/R_a ratio**	f_Z/r_e ratio	No model	Ploughing-shearing transition based
[36]	Ti-6Al-4V	R_a	f_Z, tool coating	No model	
[37]	AISI 316L	S_a	f_Z, *TRA*, BUE density	Geometric	VC correlated BUE density
[38]	Single crystal superalloy DD8	R_a	f_Z, V_C, ap	RSM	2nd order factors' interactions
[39]	IN718 by SLM	R_a	f_Z, *TRA*	Geometric	Ploughing mode not considered
[40]	AISI 316L	R_a	V_C, cutting length	No model	
[41]	Not declared	R_a	f_Z, *TRA*	Geometric	Vibration-assisted machining
[42]	Zr-based metallic glass	R_a	f_Z, *MUCT*, *TRA*, r_e, TRO	Geometric	Surface topology representation
[43]	Al6061	R_a	f_Z, *MUCT*, *TRA*, r_e	Geometric	Surface topology representation
[44]	Ti-6Al-4V	R_a	f_Z/r_e ratio	No model	
[45]	PMMA	R_a	V_C, *TA*	No model	

*_MUCT_ minimum uncut chip thickness, _TRA_ tool relief angle, r_e tool edge radius, a_p axial depth of cut, _BUE_ built-up-edge, _TRO_ tool run-out, **k_C specific cutting pressure

estimated values. Hence, by reversing Eq. (2), S_{a_SLM} can be expressed by Eq. (6).

$$S_{a\_SLM} = \frac{0.320174 \bullet e^{\frac{S_{a\_SLMnorm} - 0.392249}{0.550540}} + 0.196534}{1 + e^{\frac{S_{a\_SLMnorm} - 0.392249}{0.550540}}} \quad (6)$$

Finally, by using Eq. (3), Eq. (6), and Eq. (5), the value of S_a for each combination of process parameters, and for each manufacturing process of the specimens were calculated. The measured and estimated S_a values, with indication of the percentage error $e_{\%}$ between them, are summarized in Tables 9, 10, and 11.

Table 9 Comparison between experimental and estimated values of S_a for as-received specimens and related percentage errors in calculation

V_C	f_Z	Exp. S_a	Modeled S_a	$e_{\%}$
[m/min]	[µm/tooth*rev]	[µm]	[µm]	
40	4.0	0.36	0.369	2.4
45	3.5	0.27	0.257	4.7
35	3.5	0.29	0.452	56.0
50	3.0	0.27	0.274	1.6
40	3.0	0.37	0.351	5.2
40	3.0	0.34	0.351	3.2
40	3.0	0.35	0.351	0.3
30	3.0	0.44	0.432	1.8
45	2.5	0.37	0.378	2.1
35	2.5	0.32	0.341	6.5
40	2.0	0.39	0.378	3.2

3.5 Discussion

ANOVAs performed on the different types of specimens, produced via the three different processes described above, reveal that, regardless of the specimen preparation process, the cutting speed has a strong influence on the quality of the final part surface. In particular, when V_C is decreased, the roughness value of the machined surface increases, and, following the investigation of Kiswanto et al. [46], this can be explained by the effect of vibrations induced by the non-homogeneous properties of the material and by the formation of built-up edges at lower cutting speeds. The significance of feed rate has been observed only for SLM specimens, while its interaction with V_C appreciably affects the surface roughness of as-received samples. The influence of f_Z on components produced with SLM can be justified by the higher brittleness associated with these specimens. This feature derives from the microstructure resulting from the higher cooling rate induced by the SLM technique, which leads to a more pronounced shear cutting mode, from which traces of the tool passage remain on the surface, as observed by Gorsse et al. [47]. On the other hand, Rafi et al. [48] highlighted that due to the more ductile microstructure associated with as-received and EBM specimens, the high contribution of the ploughing mode improves surface plastic deformation by reducing path traces. Furthermore, an increase in f_Z has been indicated by Roushan et al. [49] as a reducing factor for vibrations, with a related decrease in surface roughness. Nevertheless, for better understanding the misty effect of

Table 10 Comparison between experimental and estimated values of S_a for SLM specimens and related percentage errors in calculation

V_C	f_Z	Exp. S_a	Modeled S_a	$e_{\%}$
[m/min]	[µm/tooth*rev]	[µm]	[µm]	
40	4.0	0.20	0.199	0.4
45	3.5	0.20	0.200	0.1
35	3.5	0.22	0.231	5.0
50	3.0	0.20	0.200	0.0
40	3.0	0.26	0.231	11.2
40	3.0	0.22	0.231	4.9
40	3.0	0.24	0.231	3.8
30	3.0	0.31	0.305	1.6
45	2.5	0.22	0.222	0.7
35	2.5	0.29	0.300	3.5
40	2.0	0.29	0.285	1.9

Table 11 Comparison between experimental and estimated values of S_a for EBM specimens and related percentage errors in calculation

V_C	f_Z	Exp. S_a	Modeled S_a	$e_{\%}$
[m/min]	[µm/tooth*rev]	[µm]	[µm]	
40	4.0	0.27	0.258	4.3
45	3.5	0.20	0.222	11.0
35	3.5	0.24	0.278	3.1
50	3.0	0.25	0.209	5.1
40	3.0	0.26	0.257	1.2
40	3.0	0.34	0.257	7.1
40	3.0	0.29	0.257	11.4
30	3.0	0.25	0.292	0.6
45	2.5	0.25	0.259	3.5
35	2.5	0.29	0.285	1.7
40	2.0	0.23	0.302	0.7

f_Z on both as-received and EBM samples, further analysis is mandatory.

Regarding the total surface roughness values for the different types of specimens, these values appear to be lower for SLM samples than EBM, while the highest values were observed for as-received. This can again be attributed to the different microstructures. In fact, higher ductility causes the material to adhere to the radius corresponding to the cutting-edge, negatively affecting S_a, while brittle behavior leads to less burr formation [50].

Without considering the percentage error of 56 % in Table 9, which is related to an outlier identified in the S_a measurement of as-received specimens, the maximum computational error of the mathematical models derived from RSM is around 11 % (Tables 9, 10, and 11). These outcomes highlight the reliability of the developed models when estimating the resulting micro-milling surface roughness, allowing, depending on the type of material, both to predict the achievable surface roughness value once the cutting parameters have been selected and to optimize the range of process parameters once the desired S_a value has been identified. The results of the micro-milling tests performed did not identify a combination of material, manufacturing process, and processing parameters that could achieve the required surface roughness values for optimal osseointegration for dental applications ($S_a = 1.5$ µm). Therefore, for this field of application the use of shot blasting still remains the most convenient and suitable process. Medium and low S_a values, in a range between 0.200 and 0.500 µm, are instead reachable, making micro-milling suitable for bone plates and screws, or ball joints (Fig. 1). In consideration of this, and exploiting Eqs. (3–6), a set of proposed optimized values of process parameters as a function selected values of three-dimensional surface roughness are proposed in Table 12.

However, as previously acknowledged by Kemény et al. [51], it is worth pointing out that the detection of the most suitable surface roughness value for osseointegration enhancement is also affected by surface chemistry and morphology, resulting in the need for a more complex analysis to allow optimal conditions. Moreover, different biomedical applications, such as dental or orthopedic implants, have different requirements, hence it is not possible to draw general conclusions for quantitative optimal surface roughness for all biomedical applications [52]. In general, surface roughening is beneficial for osseointegration, while a smooth surface provides higher fatigue resistance and fretting corrosion resistance [53].

Further investigation of micro-milling processes should be carried out to analyze the possibility of using only machining techniques without post-processing. However,

Table 12 Process parameters values optimized by Eqs. (3–6) for selected S_a values

	As-received		SLM		EBM	
Selected S_a	f_Z	V_C	f_Z	V_C	f_Z	V_C
[µm]	[µm/tooth*rev]	[m/min]	[µm/tooth*rev]	[m/min]	[µm/tooth*rev]	[m/min]
0.200	3.3	50	3.9	40	3.2	50
0.300	3.1	45	2.5	35	2.1	35
0.400	2.8	30	Not achievable		Not achievable	
0.500	3.3	30	Not achievable		Not achievable	

the values achieved are usable for prosthetic implants and cell cultures.

4 Conclusions

In this work, a series of mathematical models were presented for the evaluation of surface roughness aimed at improving the osseointegration of prosthetic implants, resulting from the process of micro-milling applied on parts made of Ti-6Al-4V resulting from three different manufacturing processes. These models have been derived from RSM analysis of experimental measurements of S_a three-dimensional surface roughness parameter of machined material achieved by conventional rolling process (as-received), SLM and EBM additive manufacturing techniques. To achieve this target, an extensive experimental campaign consisting of a series of micro-milling tests was carried out. Comparison between the experimental results and those calculated by the models are in good agreement, highlighting the ability of the derived equations to estimate the final surface quality. Considering the initial material conditions, the SLM samples showed higher surface roughness values than the as-received and EBM ones, and this can be ascribed to the specific microstructures resulting from the different cooling rates associated with the manufacturing technique used. SLM technique, characterized by higher cooling rates, led to a microstructure characterized by higher brittleness than that of the other specimens, thus promoting a shearing cutting mode. This particular condition produces more pronounced path traces on the machined surface with respect to materials with higher ductility, where an important contribution is given by the mechanism of the ploughing cutting. In addition, an ANOVA of the experimental results allowed the investigation among the process parameters, thus understanding which ones influence surface roughness. As a result, it was possible to show that cutting speed is the most influential parameter for all production methods, while feed per tooth has a significant impact only on SLM samples. In general, an increase of S_a has been observed when both V_C and f_Z decrease, and this is again ascribable to the microstructure-dependent cutting mechanism. However, it should be noted that further analysis will be needed to clearly assess the contribution of f_Z. Establishing the optimal surface roughness value, in fact, remains a challenging task. Indeed, it involves understanding a phenomenon that is not only a function of the manufacturing process, but also of the final implant application, the chemistry and topology of the material surface, and the mechanical and corrosion resistance properties that may affect good and durable osseointegration of the prosthesis, as summarized in Figs. 1 and 2. Consequently, in addition to the exploitation of the proposed models, further studies, and at least in-vitro osseointegration tests, are needed to identify the optimal topography that can adequately combine all requirements.

Acknowledgements The authors thank Eng. Sonja Kiem for the help provided in the data analysis and in the development of regression models.

Availability of data and material The authors declare that there are not restrictions in the availability of data and material.

Author contribution All authors contributed to the study conception and design. Material preparation, data collection, and analysis were performed by Cristian Cappellini, Andrea Abeni, Aldo Attanasio, and Alessio Malandruccolo. The first draft of the manuscript was written by Cristian Cappellini] and all authors commented on previous versions of the manuscript. All authors read and approved the final manuscript.

Funding Open access funding provided by Università degli studi di Bergamo within the CRUI-CARE Agreement.

Declarations

Conflict of interest The authors declare no competing interests.

Open Access This article is licensed under a Creative Commons Attribution 4.0 International License, which permits use, sharing, adaptation, distribution and reproduction in any medium or format, as long as you give appropriate credit to the original author(s) and the source, provide a link to the Creative Commons licence, and indicate if changes were made. The images or other third party material in this article are included in the article's Creative Commons licence, unless indicated otherwise in a credit line to the material. If material is not included in the article's Creative Commons licence and your intended use is not permitted by statutory regulation or exceeds the permitted use, you will need to obtain permission directly from the copyright holder. To view a copy of this licence, visit http://creativecommons.org/licenses/by/4.0/.

References

1. Sarraf M, Rezvani Ghomi E, Alipour S, Ramakrishna S, Sukiman NL (2022) A state of the art review of the fabrication and characteristics of titanium and its alloys for biomedical applications. Bio-des Manuf 5:371–395. https://doi.org/10.1007/s42242-021-00170-3
2. Hao YL, Li SJ, Yang R (2016) Biomedical titanium alloys and their additive manufacturing. Rare Met 36:661–671. https://doi.org/10.1007/s12598-016-0793-5
3. Heimann RB (2020) Biomaterials – characteristics, history, applications. In: Heimann RB (ed) Materials for Medical Applications, 1st edn. Walter de Gruyter, Berlin/Boston, pp 1–74
4. Buser D, Schenk RK, Steinemann S, Fiorellini JP, Fox CH, Stich H (1991) Influence of surface characteristics on bone integration of titanium implants. A histomorphometric study in miniature pigs. J Biomed Mater Res 25(7):889–902. https://doi.org/10.1002/jbm.820250708
5. Aghili SA, Hassani K, Nikkhoo M (2021) A finite element study of fatigue load effects on total hip joint prosthesis. Comput Methods Biomech Biomed Engin 24(14):1545–1551. https://doi.org/10.1080/10255842.2021.1900133
6. Rauch E, Unterhofer M, Nakkiew W, Baisukhan A, Matt DT (2021) Potential of the application of additive manufacturing technology in European SMEs. Chiang Mai Univ J Nat Sci 20(2):1–14. https://doi.org/10.12982/CMUJNS.2021.023

7. Liu S, Shin YC (2019) Additive manufacturing of Ti6Al4V alloy: a review. Mater Des 164:107552. https://doi.org/10.1016/j.matdes.2018.107552
8. Yeong WY, Chua CK (2013) A quality management framework for implementing additive manufacturing of medical devices. Virtual Phys Prototyp 8(3):193–199. https://doi.org/10.1080/17452759.2013.838053
9. Tong J, Bowen CR, Persson J, Plummer A (2017) Mechanical properties of titanium-based Ti–6Al–4V alloys manufactured by powder bed additive manufacture. Mater Sci Technol 33(2):138–148. https://doi.org/10.1080/02670836.2016.1172787
10. Sheoran AJ, Kumar H, Arora PK, Moona G (2020) Bio-medical applications of additive manufacturing: a review. Procedia Manuf 51:663–670. https://doi.org/10.1016/j.promfg.2020.10.093
11. Abeni A, Cappellini C, Ginestra PS, Attanasio A (2022) Analytical modeling of micro-milling operations on biocompatible Ti6Al4V titanium alloy. Procedia CIRP 110:8–13. https://doi.org/10.1016/j.procir.2022.06.004
12. Filiz S, Xie L, Weiss LE, Ozdoganlar OB (2008) Micromilling of microbarbs for medical implants. Int J Mach Tool Manuf 48(3-4):459–472. https://doi.org/10.1016/j.ijmachtools.2007.08.020
13. Huo D, Cheng K (2013) Overview of micro cutting. In: Huo D, Cheng K (eds) Micro-cutting fundamental and applications, 1st edn. Wiley, Chichester, West Sussex (UK), pp 3–18
14. Wennerberg A, Albrektsson T (2009) Effects of titanium surface topography on bone integration: a systematic review. Clin Oral Implants Res 20(4):172–184. https://doi.org/10.1111/j.1600-0501.2009.01775.x
15. Albrektsson T, Wennerberg A (2019) On osseointegration in relation to implant surfaces. Clin Implant Dent Relat Res 21(1):4–7. https://doi.org/10.1111/cid.12742
16. Erwin N, Debashish S, Bahar BG (2022) Remediation of machining medium effect on biocompatibility of titanium-based dental implants by chemical mechanical nano-structuring. J Mater Res 37(16):2686–2697. https://doi.org/10.1557/s43578-022-00553-x
17. Chi G, Yi D, Liu H (2020) Effect of roughness on electrochemical and pitting corrosion of Ti-6Al-4V alloy in 12 wt.% HCl solution at 35 °C. J Mater Res Technol 9(2):1162–1174. https://doi.org/10.1016/j.jmrt.2019.11.044
18. Lin L, Wang H, Ni M, Rui Y, Cheng TY, Cheng CK, Pan X, Li G, Lin C (2014) Enhanced osteointegration of medical titanium implant with surface modifications in micro/nanoscale structures. J Orthop Translat 2(1):35–42. https://doi.org/10.1016/j.jot.2013.08.001
19. Wu T, Cheng K (2013) Micro milling: the state-of-the-art approach towards applications. In: Huo D, Cheng K (eds) Micro-cutting fundamental and applications, 1st edn. Wiley, Chichester, West Sussex (UK), pp 185–226
20. Abeni A, Metelli A, Cappellini C, Attanasio A (2021) Experimental optimization of process parameters in CuNi18Zn20 micromachining. Micromachines 12(11):1293. https://doi.org/10.3390/mi12111293
21. Hacking SA, Boyraz P, Powers BM, Sen-Gupta E, Kucharski W, Brown CA, Cook EP (2012) Surface roughness enhances the osseointegration of titanium headposts in non-human primates. J Neurosci Methods 211:237–244. https://doi.org/10.1016/j.jneumeth.2012.09.002
22. Gialanella S, Malandruccolo A (2020) Titanium and titanium alloys. In: Gialanella S, Malandruccolo A (eds) Aerospace alloys, 1st edn. Springer Cham, Switzerland, pp 129–189
23. Kaliaraj GS, Siva T, Ramadoss A (2021) Surface functionalized bioceramics coated on metallic implants for biomedical and anti-corrosion performance-a review. J Mater Chem B 9(46):9433–9460. https://doi.org/10.1039/d1tb01301g
24. Pedeferri P (2018) Corrosion in the human body. In: Lazzari L, Pedeferri MP (eds) Corrosion Science and Engineering, 1st edn. Springer Cham, Switzerland, pp 575–587
25. Nicholson JW, Connor AJ (2020) Biological interactions with materials. In: Nicholson JW (ed) The Chemistry of Medical and Dental Materials, 2nd edn. Royal Society of Chemistry, pp 186–226
26. Herbster M, Rosemann P, Michael O, Harnisch K, Ecke M, Heyn A, Lohmann CH, Bertrand J, Halle T (2022) Microstructure-dependent crevice corrosion damage of implant materials CoCr28Mo6, TiAl6V4 and REX 734 under severe inflammatory conditions. J Biomed Mater Res Part B Appl Biomater 110(7):1687–1704. https://doi.org/10.1002/jbm.b.35030
27. Ginestra PS, Ferraro RM, Zohar-Haubert K, Abeni A, Giliani S, Ceretti E (2020) Selective laser melting and electron beam melting of Ti6Al4V for orthopedic applications: a comparative study on the applied building direction. Materials 13(23):5584. https://doi.org/10.3390/ma13235584
28. Men Y, Liu J, Chen W, Wang X, Liu L, Ye J, Jia P, Wang Y (2022) Material parameters identification of 3D printed titanium alloy prosthesis stem based on response surface method. Comput Methods Biomech Biomed Engin. https://doi.org/10.1080/10255842.2022.2089023
29. Montgomery DC (2019) Design and analysis of experiments, 10th edn. John Wiley & Sons, Hoboken, NJ, US
30. Concli F, Maccioni L, Fraccaroli L, Cappellini C (2022) Effect of gear design parameters on stress histories induced by different tooth bending fatigue tests: a numerical-statistical investigation. Appl Sci 12(8):3950. https://doi.org/10.3390/app12083950
31. Weule H, Hüntrup V, Trischler H (2001) Micro-cutting of steel to meet new requirements in miniaturization. CIRP Ann 50(1):61–64. https://doi.org/10.1016/S0007-8506(07)62071-X
32. Li H, Lai X, Li C, Feng J, Ni J (2008) Modelling and experimental analysis of the effects of tool wear, minimum chip thickness and micro tool geometry on the surface roughness in micro-end-milling. J Micromech Microeng 18:025006. https://doi.org/10.1088/0960-1317/18/2/025006
33. Sooraj VS, Jose M (2011) An experimental investigation on the machining characteristics of microscale end milling. Int J Adv Manuf Technol 56:951–958. https://doi.org/10.1007/s00170-011-3237-2
34. Vasquez E, Ciurana J, Rodriguez CA, Thepsonthi T, Özel T (2011) Swarm intelligent selection and optimization of machining system parameters for microchannel fabrication in medical devices. Mater Manuf Process 26(3):403–414. https://doi.org/10.1080/10426914.2010.520792
35. de Oliveira FB, Rodrigues AR, Teixeira Coelho R, de Souza AF (2015) Size effect and minimum chip thickness in micromilling. Int J Mach Tool Manuf 89:39–54. https://doi.org/10.1016/j.ijmachtools.2014.11.001
36. Aslantas K, Hopa HE, Percin M, Ucun I, Cicek A (2016) Cutting performance of nano-crystalline diamond (NCD) coating in micro-milling of Ti6Al4V alloy. Precis Eng 45:55–66. https://doi.org/10.1016/j.precisioneng.2016.01.009
37. Wang Z, Kovvuri V, Araujo A, Bacci M, Hung WNP, Bukkapatnam STS (2016) Built-up-edge effects on surface deterioration in micromilling processes. J Manuf Process 24:321–327. https://doi.org/10.1016/j.jmapro.2016.03.016
38. Gao Q, Gong Y, Zhou Y, Wen X (2017) Experimental study of micro-milling mechanism and surface quality of a nickel-based single crystal superalloy. J Mech Sci Technol 31(1):171–180. https://doi.org/10.1007/s12206-016-1218-y
39. Sadiq MA, Hoang NM, Valencia N, Obeidat S, Hung WNP (2018) Experimental study of micromilling selective laser melted Inconel 718 superalloy. Proc Manuf 26:983–992. https://doi.org/10.1016/j.promfg.2018.07.129

40. Gomes MC, Bacci da Silva M, Viana Duarte MS (2020) Experimental study of micromilling operation of stainless steel. Int J Adv Manuf Technol 111:3123–3139. https://doi.org/10.1007/s00170-020-06232-7
41. Kiswanto G, Johan YR, Poly KTJ (2020) Machined surface roughness geometry model development on ultrasonic vibration assisted micromilling with end mill. Key Eng Mater 846:122–127. https://doi.org/10.4028/www.scientific.net/KEM.846.122
42. Wang T, Wu X, Zhang G, Xu B, Chen Y, Ruan S (2020) Theoretical study on the effects of the axial and radial runout and tool corner radius on surface roughness in slot micromilling process. Int J Adv Manuf Technol 108:1931–1944. https://doi.org/10.1007/s00170-020-05492-7
43. Zhang X, Yu T, Zhao J (2020) Surface generation modeling of micro milling process with stochastic tool wear. Precis Eng 61:170–181. https://doi.org/10.1016/j.precisioneng.2019.10.015
44. Bhople N, Mastud S, Satpal S (2021) Modelling and analysis of cutting forces while micro end milling of Ti-alloy using finite element method. Int J Simul Multidisci Des Optim 12(26). https://doi.org/10.1051/smdo/2021027
45. Geng Y, Zhang S, Wang J, Xiao G, Li C, Yan Y (2023) Effect of inclined angle of micromilling tool on the fabrication of the microfluidic channel. Int J Adv Manuf Technol 125:3069–3079. https://doi.org/10.1007/s00170-023-10958-5
46. Kiswanto G, Mandala A, Azmi M, Ko TJ (2020) The effects of cutting parameters to the surface roughness in high speed cutting of micro-milling titanium alloy ti-6al-4v. Key Eng Mater 846:133–138. https://doi.org/10.4028/www.scientific.net/KEM.846.133
47. Gorsse S, Hutchinson C, Gouné M, Banerjee R (2017) Additive manufacturing of metals: a brief review of the characteristic microstructures and properties of steels, Ti-6Al-4V and high-entropy alloys. Sci Technol Adv Mater 18(1):584–610. https://doi.org/10.1080/14686996.2017.1361305
48. Rafi HK, Karthik NV, Gong H, Starr TL, Stucker BE (2013) Microstructures and mechanical properties of Ti6Al4V parts fabricated by selective laser melting and electron beam melting. J Mater Eng Perform 22(12):3872–3883. https://doi.org/10.1007/s11665-013-0658-0
49. Roushan A, Srinivas Rao U, Patra K (1950) Sahoo P (2012) Multi-characteristics optimization in micro-milling of Ti6Al4V alloy. J Phys: Conf Ser 1:012046. https://doi.org/10.1088/1742-6596/1950/1/012046
50. Kumar SPL, Avinash D (2019) Experimental biocompatibility investigations of Ti–6Al–7Nb alloy in micromilling operation in terms of corrosion behavior and surface characteristics study. J Braz Soc Mech Sci Eng 41(9):364. https://doi.org/10.1007/s40430-019-1858-9
51. Kemény A, Hajdu I, Károly D, Pammer D (2018) Osseointegration specified grit blasting parameters. Mater Today: Proc 5(13):26622-26627. https://doi.org/10.1016/j.matpr.2018.08.126
52. Krishna Alla R, Ginjupalli K, Upadhya N, Shammas M, Krishna Ravi R, Sekhar R (2011) Surface roughness of implants: a review. Trends Biomater Artif Organs 25(3):112–118
53. Lopez-Ruiz P, Garcia-Blanco MB, Vara G, Fernández-Pariente I, Guagliano M, Bagherifard S (2019) Obtaining tailored surface characteristics by combining shot peening and electropolishing on 316L stainless steel. Appl Surf Sci 492:1–7. https://doi.org/10.1016/j.apsusc.2019.06.042

Publisher's note Springer Nature remains neutral with regard to jurisdictional claims in published maps and institutional affiliations.